SEPARATION OF CONVECTIVE AND STRATIFORM PRECIPITATION IN MESOSCALE SYSTEMS

NIMBOSTRATUS clouds are produced by thermodynamically stable air motions and are deep enough to allow precipitation particles to grow to the sizes of raindrops and snowflakes. Widespread vertical air motions are essential to the production of nimbostratus. One way that nimbostratus cloud occurs is adjacent to and dependent on the outflow from active deep convective clouds. In other cases, nimbostratus may be the residue of earlier active deep convective clouds. To understand deep precipitating clouds, it is often important to separate the active convection elements from the rest of the nimbostratus cloud. We refer to such analysis as *convective/stratiform separation*

1. Definition of stratiform precipitation and how it differs from convective precipitation

Precipitation is of two clearly distinguishable types—*stratiform* and *convective*. Stratiform precipitation falls from nimbostratus clouds, while convective precipitation falls from active cumulus and cumulonimbus clouds. These cloud types may occur separately or entangled with each other in the same cloud complex. Figure 1 compares the salient features of these two basic types of cloud and precipitation. Although our present purpose is to examine stratiform precipitation, it is essential to define both convective and stratiform precipitation, because the definitions are better understood in contrast with each other, and because convective and stratiform precipitation are typically present together.

It is possible for warm stratiform clouds (tops below 0°C level) to produce precipitation. Stratus and stratocumulus may produce drizzle. When low-level warm stratiform clouds are a little deeper or more vigorous they may produce some light rain. However, by far the bulk of stratiform precipitation falls from nimbostratus clouds that reach well above the 0°C level and contain ice particles. With this fact in mind, we find it most convenient to define stratiform and convective precipitation kinematically, in terms of the vertical air motion relative to the fallspeed of ice particles. The precipitation process in most deep nimbostratus clouds depends of the ability of ice hydrometeors to grow while drifting slowly downward. Stratiform precipitation may therefore be defined as a process in which the vertical air motion is *generally* small compared to fall velocity of ice crystals and snow. More specifically, precipitation is defined to be stratiform if the mean vertical velocity of the air w averaged over an atmospheric volume containing stratiform precipitation satisfies the condition:

$$0 < \left|\overline{w}\right| \ll V_{\text{ice, typical}} \tag{1}$$

where $\overline{w}$ is the vertical motion averaged over a region containing stratiform precipitation, and $V_{\text{ice, typical}}$ represents the typical terminal fall velocity of ice crystals and

snow (usually in the range of ~1-3 m s^{-1}). When the mean vertical velocity lies in the range (1), the air motions cannot disrupt the general downward drift of ice particles. It is important that (1) refers to the *average* vertical air motion in the nimbostratus because it is common for the nimbostratus to contain small pockets of vertical motion where the local value of *w* exceeds the ice-particle velocity scale. The existence or non-existence of stratiform precipitation should therefore be decided only in the averaged sense and not on the basis of local values of *w*.

Stratiform precipitation has two important subtypes that both satisfy (1) but are physically and dynamically distinct. An active stratiform region is defined for which the air motion is overall upward, so that (1) is being satisfied by the more stringent condition

$$\left|\overline{w}\right| \ll V_{\text{ice, typical}} \text{ , and } \overline{w} > 0 \qquad \text{(1a)}$$

The overall positive average vertical air velocity allows ice particles to grow by deposition while yet being heavy enough to fall relative to the Earth's surface through the generally slowly upward moving air.

An *inactive stratiform region* is one in which the mean vertical velocity satisfying (1) is overall downward, i.e.

$$\left|\overline{w}\right| \ll V_{\text{ice, typical}} \text{ , and } \overline{w} \le 0 \qquad \text{(1b)}$$

In this case the precipitation particles in the stratiform region in which the averaging applies do not grow on average and may even lose mass if the mean air motion is downward. This type of stratiform precipitation is sometimes characterized as "debris" or "fallout."

The active type of stratiform precipitation process in deep nimbostratus containing ice particles aloft is depicted schematically in Figure 1a. Precipitation particles that eventually fall to the ground as raindrops have their early history as ice particles in the upper parts of the cloud. We will defer discussion of the important question of *how* these particles first appear in the upper reaches of the cloud. For now, we note only that they may form *in situ*; they may be introduced from a source located to the sides of or above nimbostratus; or they may originate from a source embedded within the cloud itself. Once introduced into the nimbostratus cloud, the ice particles begin to grow. The positive vertical air velocity maintains supersaturation and deposition of vapor onto the ice particles. According to (1a), the mean vertical velocity of the air $\overline{w}$ must be positive and large enough to maintain supersaturation; however, it must small enough not to violate $\left|\overline{w}\right| \ll V_{\text{ice, typical}}$. It is important to note that in general the ice particles in the upper levels of nimbostratus *are falling*; they are not suspended or carried aloft by the air motions as they grow, except occasionally by an embedded local pocket of updraft that might temporarily advect particles upward. Thus, the average in-cloud vertical air motion in pure nimbostratus conforms to (1a), not exceeding a few tens of centimeters per second, allowing particles to fall while continuing to support the growth of the falling ice particles by vapor deposition.

The higher the altitude at which the ice particles are formed or introduced from an outside source, the longer they will be able to grow by deposition of the vapor made available as a result of mean upward air motion in the nimbostratus. The time available for growth of the ice particles falling from cloud top is ~1-3 h (the time it takes a particle falling at ~1-3 m s^{-1} to descend 10 km). This amount of time is sufficient for the particles to grow by deposition to moderately large size. When the ice particles falling and growing by deposition descend to within about 2.5 km of the 0°C level, aggregation and riming can occur, allowing the particles to achieve still larger size. Most importantly, the particles begin to aggregate and form large, irregularly shaped snowflakes. The particles may even grow by riming, since at these warmer levels, the vertical air motions of a few tens of centimeters per second are sometimes strong enough to maintain a small number of liquid-water drops in the presence of the falling ice particles. Aggregation becomes more frequent within about 1 km of the 0°C level. Aggregation does not add mass to the precipitation but rather concentrates the condensate into large particles, which, upon melting, become larger, rapidly falling raindrops. As will be explained below, the layer in which the large snowflakes melt is marked on radar by a *bright band* of intense echo in a horizontal layer ~0.5 km thick, located just below the 0°C level. The bright band produced by melting particles and other characteristics of vertical structure of the radar echo in stratiform precipitation are particularly informative about the dominant precipitation mechanisms in the nimbostratus and will be discussed in more detail in Section 2.

The convective precipitation process is depicted in Figure 1b. Its radar echo pattern contrasts sharply with that of stratiform precipitation. The radar echo maxima form vertically oriented columns rather than the horizontal layers produced by the bright band in the stratiform precipitation case. In the convective precipitation process, condition (1) is not met. Instead the mean vertical air velocity at a given height in the updraft zone has a magnitude of $\overline{w} \sim 1-10$ m s^{-1}, which equals or exceeds the typical fall speeds of ice crystals and snow.

Observations show that the time available for the growth of precipitation particles in convective precipitation is limited; often rain reaches the ground within a half hour of cloud formation. This time is much shorter than the 1-3 h available for growth of precipitation particles in a stratiform cloud deck.[1] Since the time for growth is so short,

---

[1]The idea of distinguishing convective from stratiform precipitation on the basis of the magnitude of the in-cloud vertical air motion and time scale of the microphysical precipitation growth process was suggested by the pioneering cloud physicist Henry Houghton, in one of his last papers (Houghton, 1968). Houghton's distinction captures the physical essence of the two precipitation types. The early radar meteorologist Louis Battan further articulated differences between convective and stratiform entities in terms of their radar-observed structures in his textbooks on meteorological radar (Battan, 1959, 1973). He called the two types of precipitation "convective" and "continuous," the latter

the precipitation particles must originate and grow not far above cloud base at the time the cloud forms (time t_o in Figure 1b). It is possible for the growth to begin at that time since updrafts in the convective elements are strong enough to carry the growing particles upward until they become heavy enough to overcome the updraft and begin to fall relative to the ground (see the particle trajectory in Figure 1b). The only microphysical growth mechanism rapid enough to allow the particles to develop this quickly is accretion of liquid water. In contrast, accretion of liquid water is at most of minor importance in stratiform precipitation, where the dominant microphysical mechanisms are vapor, deposition, and aggregation of ice particles. Since the strong convective updrafts carrying the particles upward during the growing phase of the cloud condense large amounts of liquid water, the large particles (whether liquid or ice) in the rising parcels of air can grow readily by accretion of cloud liquid water. Aircraft observations of ice particles in convective clouds confirm that the particles in the updrafts grow largely by riming. Since the strong updrafts in convective clouds are usually narrow (typically a few km or less in width), radar echoes from precipitation associated with active convection form well-defined vertical cores of maximum reflectivity.

In the dissipating stages of precipitating clouds (after t_5 in Figure 1b), strong upward motions cease and no longer carry precipitation particles upward or suspend them aloft. The fallout of particles left aloft by the dying updrafts can then take on a stratiform character, including a radar bright band. Indeed, large regions of stratiform precipitation can form when clusters of convective cells die out in a given region.

2 The contrasting radar-echo structures of stratiform and convective precipitation

The schematic in Figure 1a depicts qualitatively the radar-echo structure of a zone of active stratiform precipitation satisfying (1a), with the melting layer denoted by the radar bright band being the most prominent feature. Closer, quantitative examination of the vertical profile of radar data in stratiform precipitation allows us to divide the precipitation into distinct layers in which different microphysical processes dominate. These layers are bounded by points 0-4 in Figure 2.

The zone from 0 to 1 in Figure 2 is associated primarily with ice particles growing by *vapor deposition*, which is the slowest microphysical growth mode. Since the ice particles settling downward through the nimbostratus do not grow rapidly, the equivalent radar reflectivity Z_e, which is proportional to the sixth moment of the particle size distribution, does not increase rapidly with decreasing altitude between 0 and 1. In the layer between 1 and 2, the particles continue to grow by deposition and possibly some

---

corresponding to stratiform precipitation in our terminology. In describing continuous precipitation, he emphasized the radar bright band, the existence of embedded non-uniform echo structure, and the continuous precipitation, and how convective echoes take on a bright band structure in their late stages. The views depicted in Figure 6.1a and b are largely a combination of those of Houghton and Battan.

riming. However, they also undergo aggregation with increasing frequency as they approach the melting layer. The aggregation has the effect of producing very large particles. Since Z_e depends on the sixth power of the particle dimension, the formation of these large particles sharply increases the radar reflectivity between levels 1 and 2.

The changes in the radar reflectivity profile between levels 2 (the 0°C level) and 4 are all associated with *melting*. The center of this layer (level 3) is marked by a sharp maximum of Z_e, which gives the melting layer its identity as the bright band. Several processes strongly affect the radar reflectivity profile in the melting layer. The sharp increase in the radar reflectivity downward from levels 2 to 3 is thought to be the result of two effects. First, aggregation continues to occur, as in the layer from 1-2. This conclusion is arrived at inductively, since other effects cannot fully explain the increase in reflectivity factor from points 2 to 3. A second significant effect on Z_e is that the magnitude of the complex index of refraction of the particles [$|K|^2$]changes as they melt from 0.197 (for ice particles) to 0.93 (for liquid water drops). If in the first stage of melting, the particles take on the character of water but do not collapse to form smaller drops until the end of the melting process, then *Z*, which is proportional to the sixth moment of the particle size distribution, remains constant. However, Z_e increases by a factor of $0.93/0.197 \approx 5$ since $Z_e = \left(|K|^2 / 0.93\right) Z$. As noted above, this amount of increase in Z_e between points 2 and 3 is insufficient by itself to fully explain the magnitude of the peak of reflectivity in the bright band, and it is for this reason that it is thought that the aggregation acts in concert with the index of refraction change to produce the peak at 3.

Two effects produce the sharp dropoff of Z_e in the lower portion of the melting layer between levels 3 and 4. If the melting is completed at point 3, and all the particles collapse to form small raindrops, two things happen to Z_e. First, the particles are now smaller; therefore Z_e is lower in accordance with the sixth power of all the particle diameters. Second, the fall speed of the particles suddenly increases from $\sim$1-3 m s^{-1} for snow to $\sim$5-10 m s^{-1} for raindrops. If the downward flux of precipitation mass is the same at levels 3 and 4, as it would be in steady stratiform rain, then the mean concentration of rainwater (mass of water per volume of air) must decrease sharply from level 3 to level 4. Since the concentration of rainwater mass is the third moment of the drop size distribution and Z_e is proportional to the sixth moment of the distribution, the decrease in mass concentration between levels 3 and 4 corresponds to a decrease in Z_e through the same layer.

The layer below point 4 in Figure 2 is characterized by rain. The microphysical processes that can occur in this lowest layer are quite varied and depend on the meteorological context. In some cases, the precipitation particles in this lower region simply fall to the ground with a constant mass flux. In other cases, the rain falls through a

lower layer of cloud being continually regenerated by upward air motion, and the raindrops falling below the melting layer continue to grow by vapor diffusion and collection of cloud droplets so that the mass flux increases with decreasing height. In still other cases, the rain falling out of the melting layer falls into a layer of dry air into which the drops partially evaporate. Thus, the flux of rain reaching the surface is less than that exiting the melting layer, and the air below the melting layer is cooled by the evaporation. The cooling of the air both by this evaporation and by the melting can have important feedbacks to cloud and storm dynamics.

3 Microphysical observations in nimbostratus and implied vertical air motions

Observations of the sizes and shapes of precipitating ice particles above the 0°C level have been made aboard research aircraft flying in nimbostratus associated with mesoscale convective systems, fronts, and hurricanes, with extensive active stratiform precipitation areas. These *in situ* measurements verify the microphysical layering of the cloud that we have inferred from the radar echo profile depicted in Figure 2. An example of data obtained in nimbostratus associated with tropical mesoscale convective systems is shown in Figure 3. Particles were observed at flight levels ranging in temperature from −23° to +4°C . Two-dimensional images in the form of shadows were formed by the ice particles as they flowed through a laser-illuminated space under the wing of the aircraft. The crystalline structures of most of the images seen by this device are impossible to determine. However, occasionally a definable particle shape is discernible. The frequency with which particles of various types could be recognized was noted and plotted as a function of flight-level temperature.

The particle types indicated in Figure 3a and b (needles, columns, plates, and dendrites) are known to grow at certain ambient temperatures. If the observed particles fell about $\sim$0.5-1.0 km from their altitude of growth before being encountered by the aircraft,[2] then their growth temperature (T_G) would be expected to be $\sim$3-6°C lower than the flight-level temperatures indicated in Figure 3. Taking this difference into account, we see that the maxima and minima of the curves in Figure 3a and b for needles, columns, plates, and dendrites all occur at flight-level temperatures that are consistent with having fallen from levels corresponding to their vapor depositional growth temperatures. This result indicates that, as we concluded from the radar-echo profile shown in Figure 2, growth of ice particles by vapor diffusion occurs above the 0°C level. Some riming could also have been occurring, as riming would be consistent with the unidentifiable shapes of many of the particle images. In Figure 3c, it can be seen that the frequency of large aggregates of crystals exhibits a broad maximum strongly overlapping with the peak of frequency of dendritic crystals seen in Figure 3b. This result is consistent with aggregation becoming more frequent as the downward-settling crystals approach the 0°C level. In addition, it appears that a primary aggregation mechanism, at least in the stratiform regions of tropical mesoscale convective systems represented by these particular data, is the arms of the dendrites becoming entangled as the ice crystals drift

---

[2]This amount of downward displacement of ice particles would require only 5-15 min at fall speeds of 1-3 m s^{-1}.

downward. The nearly round particles indicated in Figure 3c increase in frequency suddenly as the ice particles melt and form raindrops below the 0°C level.

The microphysical picture of nimbostratus indicated by the *in situ* data summarized in Figure 3 is the same as that inferred from the vertical profile of radar reflectivity in Figure 2. The region above the melting layer is characterized by particles growing by vapor diffusion and drifting downward. Some riming could occur along with the vapor diffusion, if the vertical motion becomes strong enough to condense enough water to maintain the air at saturation with respect to liquid water. Riming is most likely to occur just above the 0°C level, since the vapor content of the air increases exponentially with decreasing altitude. Although the vertical air motions might become large enough to allow some riming to occur along with the vapor diffusion, they must remain weak enough to allow the particles to continue to fall [i.e., condition (1) must remain satisfied to explain the observations]. As the particles settle downward, aggregation produces large ice particles within ~ 2-2.5 km of the top of the melting layer, with the most aggregates being found within 1 km of the 0°C level. What this structure implies about the dynamics of the nimbostratus is that there must be widespread gentle uplift of the air throughout the region of the cloud above the 0°C level. This ascent must be strong enough to supply vigorous growth by vapor diffusion (and possibly some riming), but weak enough to allow for the sedimentation of the ice particles. Since these particles fall at speeds ~ 1 m s^{-1} , it is readily concluded that nimbostratus must have typical vertical velocities of a few to a few tens of centimeters per second; i.e. (1) is satisfied.

4 Role of convection in regions of stratiform precipitation

Stratiform cloud decks with gentle mean ascent satisfying (1a are seldom isolated from convection. Rather, convective cells are typically either embedded within or adjacent to the stratiform cloud layers. Thus, the dynamics of active nimbostratus are not solely a matter of gentle ascent over a wide area. Instead, there exists a symbiotic relationship in which both strong convective-scale vertical motions and widespread ascent play a role. How the convection is important to the nimbostratus is seen by further consideration of the microphysical and kinematic processes in the stratiform precipitation.

Precipitation particles that fall to the ground from the nimbostratus grow by vapor deposition at upper levels (between levels 0 and 1 in Figure 2) if the vertical motions satisfy the condition (1a) defining an active stratiform precipitation region. We have not yet considered the *origin* of these particles. The radar and aircraft instrumentation, which indicate the orderly and distinct physical profiles in Figure 2 and 3, detect particles only after they have formed and reached certain threshold sizes. Nucleation of ice particles certainly occurs readily at the upper levels of the nimbostratus cloud, since the temperature is low enough for primary nucleation of ice crystals to be active. However, it is difficult to envision nimbostratus in which nucleation of particles in the upper levels of the cloud is the only source of ice particles that grow to precipitation size and fall out of the cloud. The stratiform precipitation areas of nimbostratus are often limited in horizontal extent, and there is usually a relative wind blowing through the cloud. Growth

of recently nucleated crystals by vapor diffusion, moreover, is a rather slow process.[3] Thus, there is a tendency for the ice particles nucleated within the nimbostratus itself to be advected across the cloud before they can grow to a large-enough size to contribute to the precipitation reaching the ground below the cloud. The efficacy of the precipitation process within the nimbostratus clearly would be enhanced by any mechanism that sped up the early growth of the particles.

Convection is such a mechanism. The stronger vertical motions in even the smallest of convective updrafts can produce precipitable particles relatively quickly since large concentrations of water substance are condensed, and riming and aggregation are quickly established in the convection. If particles produced and grown to precipitable size in convection are transferred into the upper levels of a nimbostratus cloud, they do not have to first grow slowly to precipitation size in the gentle uplift in an active stratiform cloud deck but can immediately begin their descent down through the stratiform cloud layer, growing further and changing phase by the sequence of processes discussed in connection with Figure 1a, Figure 2, and Figure 3. Thus, convection can serve as a major *source* of pre-grown ice particles, which *subsequently* fall out of the nimbostratus in the orderly pattern indicated by these figures.

5. Stratiform precipitation produced by discrete redevelopment of deep convection

Precipitating ice particles can be introduced into the upper levels of nimbostratus by deep convection. Illustrated in Figure 4, this relationship between convection and nimbostratus differs greatly from shallow-layer embedded cells. As a buoyant updraft parcel rises through a deep layer, it expands because of decreasing pressure, so that the horizontal extent of the updraft element is greater at upper than at lower levels. As indicated in Figure 1, particles grow by collection (coalescence, riming, or aggregation) as they are carried up by the convective updraft. The heavier precipitation particles that grow quickly by collection exit the buoyant element at lower levels and fall into a relatively narrow horizontal zone. They constitute the bulk of the precipitation shower from the convective cell. However, when the updraft element is near the top of its ascent, ice particles are being sown into a broader horizontal area below the widened element. The net effect is like a fountain (Figure 5), with the heavier particles falling out from low levels near the updraft and the lighter particles being carried upward and outward and falling over a wider area around the convective updraft.

When several deep updrafts occur near each other (Figure 5), the spreading upper portions of the particle fountains merge at upper levels, producing an intermediary region of lighter precipitation and weaker radar echo between the narrow concentrated rain areas of large particles falling from the lower portions of the cells. The result on radar is a zone of echo characterized by vertically oriented cores of high reflectivity embedded within surrounding weaker echo within a larger, mesoscale region containing the group of

---

[3]At the relatively warm temperature of -5°C, a small ice particle can grow by deposition to drizzle size in ~1/2 h, but after that its growth rate slows down (Wallace and Hobbs, 2006).

convective cells (Figure c). The intermediary light precipitation might exhibit a bright band due to the falling ice particles from the upper portions of the particle fountains. However, this intermediary zone between active cells often satisfies (1b), not (1a), because $\overline{w} \leq 0$ as a result of the compensatory downward and/or near-zero vertical motion in the regions between the cells. In this case the light precipitation due to particle fountain fallout between the cells is the inactive type of stratiform precipitation defined in Section 1.

In Figure 5, the downward motions indicated immediately outside the buoyant elements represent air motions that occur outside the buoyant element as part of the environment's response to the rising element. Pressure forces outside the buoyant elements drive air into their wakes to conserve mass during their upward acceleration. As the parcels' buoyancy decreases, the updrafts and surrounding downdrafts lose strength, and the upper levels of the regions containing the convection become a mixture of weak up and down motions (Figure 6a). Observations show that the mean vertical motion is positive but weak enough that it satisfies (1). Ice particles are therefore no longer advected upward at this stage, except in isolated residual pockets of slightly more active convection. Rather, the particles drift slowly downward growing by diffusion, aggregation, and some riming until they reach the 0°C level (Figure 6b). Just below that level, they melt and produce a bright band on radar (Figure 6c). As discussed in Section 2, the bright band is the classic signature of stratiform precipitation. In this way, a region of deep convection evolves into a region of stratiform precipitation; a convective region observed on radar, as illustrated schematically in Figure 5c thus evolves into a stratiform region like that shown in Figure 6c. The latter figure panel shows the bright band somewhat broken up and irregular, which is typical because the stratiform precipitation originated from a heterogeneous pattern of convective cells and consists in this later stage of previously active cells in various stages of decay. Some of the dying cells take the form of generating cells with fallstreaks if the sedimentation of ice particles from old forms trails shaped by wind shear in the precipitating region.[4]

Stratiform precipitation formed from hydrometeors produced initially in deep convective cells occurs in a wide variety of configurations determined by the local environmental wind shear, spatial variability of humidity, thermodynamic stratification, and proximity to triggering mechanisms (topography, fronts, dry lines, etc.). These organizing factors often lead to the convective elements systematically lying on one edge or another of the stratiform precipitation region, in which case the cloud and precipitation structure develops as illustrated in Figure 7. All the panels in the figure are considered to be in a coordinate system moving with the clouds. Moreover, the convective and stratiform clouds and their attendant precipitation are all assumed to be moving with a constant horizontal speed relative to the ground at all levels (i.e., there is no horizontal air motion relative to the coordinate system at any altitude). This situation applies only if

[4] Yuter and Houze (1997) show some examples of fallstreaks embedded in stratiform regions of tropical mesoscale convective systems as seen by a high resolution radar on an aircraft flying near the melting level

there is no vertical shear of the horizontal wind in the region of the clouds.[5] As was pointed out in Figure 1b, a precipitating convective cell, originally characterized as a local, intense, vertically oriented precipitation core, evolves into a stratiform structure (indicated by a radar bright band) in its later stages. It follows that if all of the convective cells initially arranged in a group at a time t_o (e.g., Figure 7a and b) weaken more or less simultaneously, then by some later time, $t_o + \Delta t$, the whole region of convection turns into a stratiform precipitation area composed of the dying remains of the earlier convective cells, as shown in the right-hand portions of Figure 7c and d. If during the same interval of time a new group of convective cells forms as shown in the left-hand portions of Figure 7c and d, then the overall cloud structure becomes that depicted in Figure 7d—a combination of cumulonimbus and nimbostratus, with cumulonimbus situated to the side of the stratiform region. The right-hand side of the cloud (between A and B) is nimbostratus that has formed from the weakening of the original convection, while the left-hand side (between B and C) is composed of new cumulonimbus. If the new convection at $t_o + \Delta t$ subsequently weakens and evolves into nimbostratus and another region of convection forms farther to the left, then the cloud and precipitation structure at time $t_o + 2\Delta t$ is that shown in Figure 7e and f. The region on the far right (between A and B) is composed of the oldest nimbostratus formed from the original convection, the middle region (between B and C) is new nimbostratus formed from the weakening of the convection at time $t_o + \Delta t$, and the region on the far left (between C and D) consists of the newest cumulonimbus.

In this way, a rather wide region of nimbostratus can form, as each successive new group of convective cells weakens and becomes part of the stratiform zone. The nimbostratus formed in this way is characterized by active stratiform precipitation maintained for a long time by widespread mean ascent throughout the upper levels of the nimbostratus that satisfies (1a). The widespread upward air motion that maintains the nimbostratus in this idealized picture is the effect of the small but positive buoyancy of the air in the tops of the cumulonimbus that weaken to form the stratiform cloud. The air rises rapidly enough to provide moisture for the growth of the ice particles, but slowly enough that the particles readily drift downward toward the melting layer and the ground. In this case, though, the precipitating ice particles are generated and grow to precipitable size during the cumulonimbus phase of the cloud. When the cumulonimbus dies and takes on a stratiform character, precipitating ice particles are already present. Since they thus exist at the onset of the nimbostratus phase, they do not need to be nucleated and grown to precipitable size in the stratiform cloud itself. The history of three ice particles is indicated schematically in Figure 7. Particle 1 is near the top of a convective cell at time t_o (Figure 7b). It has been formed at lower levels and grown to precipitable size

---

[5]The assumption of absolutely no shear here ignores the small horizontal wind components required by mass continuity to compensate for the vertical air motions in the cloud system. This slight inconsistency is not serious for this qualitative discussion, as these small horizontal components would only slightly modify the idealized picture developed in this illustration.

while being carried up to high levels by the strong convective updraft in the cumulonimbus. When the convective updrafts weaken, the particle begins to settle downward through the more gentle ascent in the upper levels of the nimbostratus. By $t_o + \Delta t$, it has reached a level midway between cloud top and the melting level, as indicated in Figure 7d. This point is directly below the position of the particle at t_o in the schematic, where the coordinate system moves with the clouds and precipitation, and there is no vertical wind shear. In the meantime, ice particle 2 has been generated in the new convection between B and C and has arrived at upper levels. When the convection between B and C weakens, the second particle falls in the same manner as the first one. By time $t_o + 2\Delta t$, it has fallen midway through the upper cloud within the region of newer nimbostratus. Particle 1 meanwhile has fallen further and is located just above the melting level at this time (Figure 7f). Particle 3 has appeared at the top of the most recent convection (between C and D) and will fall in a pattern similar to particles 2 and 3 when this region of convection weakens.

6. Stratiform precipitation produced by deep convection in sheared configurations

From the positions of particles 1, 2, and 3 in Figure 7f, we see that precipitable-sized ice particles generated and carried aloft in the updrafts of deep convective cells enter the nimbostratus at upper levels and slowly settle downward in the upper layers of the nimbostratus until they reach the melting level. In the case of no wind shear, there is no relative air motion across the cloud system, and the trajectory of each particle is therefore vertically downward in the coordinate system moving with the cloud. However, it is common for the systematic discrete redevelopment of convection illustrated in Figure 7 to occur in the presence of wind shear. Figure 8 illustrates one way in which wind shear can lead to the storm structure seen in Figure 7f. The picture assumes that convective cells and their associated particle fountains are successively regenerated to give a storm motion toward the lower right of the figure. As drawn here, the sheared airflow advects the convective elements to the rear of the line moving line as they rise. At the uppermost levels of each parcel's rise, the laterally expanded and precipitating buoyant parcel remnants become the raw material of the precipitating stratiform cloud deck, seeding the upper levels of the stratiform cloud with ice particles aloft. Thus, ice particles need not be nucleated anew at upper levels; the ice particles that fall through the stratiform cloud deck have been pre-grown to precipitable size in vigorous updrafts of the previously active buoyant convective parcels. In this configuration, the ice particles labeled 3, 2, and 1 in Figure 7f can be regarded as successive positions of the same particle, i.e. a trajectory of a single particle which is generated within the updraft of the deep convection while being advected horizontally rearward into the nimbostratus cloud. The sloping trajectory connecting the points 3, 2 and 1 would then be the combined result of the horizontal relative air motion and the fall speed of the ice. This interpretation contrasts with the case of no shear, where the points 3, 2, and 1 were the locations of different particles in separate convective cells at different stages of development.

The arrangement of regenerating convective cells in a sheared environment illustrated by Figure 8 occurs very commonly. However, other shear configurations

combined with successive regeneration of convective cells lead to other patterns of convective cells juxtaposed with stratiform precipitation. For example:

- One special case is a degenerate form of the no-shear case, which occurs when the original group of convective cells (Figure 7a and b) dies out with no new area of cells subsequently generated, and the stratiform precipitation at time $t_o + \Delta t$ is thus not actually accompanied by new convection, as shown in Figure 7b, but rather appears as a region of pure nimbostratus, unaccompanied by convection. It should be remembered, though, that the particles falling from the nimbostratus in this degenerate case were generated in the earlier convection, and the process remains exactly the same as if the convection had regenerated and continued to be present alongside the nimbostratus.

- Another case occurs in the sheared mode, when the horizontal relative flow at upper levels in a case like Figure 8 is especially strong. In this situation, the stratiform and convective regions of Figure 7f become separated by a horizontal gap. Figure 9 schematically illustrates this type of structure. The heavier stratiform precipitation, resulting from the bulk of the particles falling from the upper portions of the convective cells is characterized by a robust bright band and separated from the convective cells by a zone or gap of weak radar echo. The winds at upper levels are strong enough to carry the slowly falling ice particles far enough downstream to produce the radar-echo gap.[6]

- In some cases, rapidly moving convective cells advected by lower-level winds may collide with and become incorporated into a pre-existing precipitating stratiform cloud produced by deep convection in another region. Figure 10 illustrates how this type of storm structure occurs over the near-equatorial Indian Ocean, where strong easterlies overlie low-level westerlies.[7]

7. Microphysics of the stratiform precipitation associated with deep convective clouds

Figure 1 qualitatively suggests the layering of the predominant microphysical processes within all nimbostratus clouds. Figure 6 postulates more specifically how this layering of the microphysical processes occurs within nimbostratus evolving from previously vigorous deep convection. Here we present modeling evidence of this microphysical pattern in stratiform precipitation associated with deep convection in a model simulation of a storm having the structure illustrated schematically in Figure 9. The schematic indicates that the primary mechanism of ice particle growth in the convective updrafts is riming. After the particles are advected into the stratiform region, the dominant process adding mass to the particles in the layer 0 to –12°C is vapor

[6] The spatial gap between a convective region and stratiform region was first noted by Ligda (1956) and described in detail and interpreted physically by Biggerstaff and Houze (1993) and Braun and Houze (1994).
[7] See Yamada et al. (2010) for details.

deposition, made possible by the widespread ascent at upper levels. Below about the –12°C, aggregation produces larger-sized particles but does not increase the total mass of the precipitation. Riming may add some mass to the precipitating particles in this layer, especially just above the melting level. After the particles melt, they fall through a layer of subsiding air. The raindrops evaporate partially as they fall through this lower layer.

The microphysical processes shown in the schematic were determined by Doppler-radar measurements and set to be constant in the calculations. The two-dimensional thermodynamic and bulk microphysical water-continuity equations were integrated until the fields reached a steady state. The convective region is imagined to have been providing the region with precipitating ice particles across the lateral boundary of the domain containing the nimbostratus. The horizontal wind and vertical air motion derived from Doppler radar are shown in Figure 11. The flow was generally from right to left across the domain, as in the schematic of Figure 8 so that the cloud ice and snow produced in the convective region was advected into and across the stratiform region. The upward air motion at upper levels provided an environment in which the ice particles entering the domain from the convective region could grow before they fell to the 0°C level (between 3- and 4-km altitude in this case). The steady-state distributions of q_s, q_g, and rain-water mixing ratio q_r are shown in Figure 12. The patterns in Figure 12a and b occurred by the less dense snow sweeping out and accreting the more dense snow. The sloping path of the fallout of the latter is evident in Figure 12b. When the more dense snow reaches the melting level, the highest concentration of q_g seen in Figure 12b lies between horizontal coordinates –70 and –90 km. This snow then melts and falls out rapidly, such that the heaviest concentration of rainwater at lower levels occurs between these same coordinates (Figure 12c). Figure 13 confirms that the maximum precipitation rate and radar reflectivity correspond to the fallout pattern of the more dense snow and rain. Thus, the *location* of the heaviest precipitation from the nimbostratus is determined by the pattern of fallout of snow produced in the convective region.

Although the location of the heaviest precipitation from this type of nimbostratus is determined by the fallout trajectories of the snow produced in the neighboring convection, the *amount* of precipitation that falls from the stratiform cloud is determined by a combination of effects. The convection produces the initial mass of snow entering and falling through the nimbostratus. As this snow falls through the deep stratiform cloud layer, it attains greater mass by the deposition of vapor (Figure 14a and b) before it melts (Figure 14c) and partially evaporates as it falls through the region of descent below the melting layer (Figure 14d). Comparison with data shows that the model produced an amount of stratiform precipitation consistent with observations.

Two further experiments with the numerical simulation show significant results: In the first experiment, the vertical velocity was set to zero instead of the field shown in Figure 11b. In this case, the general pattern of precipitation remained qualitatively the same, but the total mass of rain reaching the surface decreased by a factor of four. Although the ice particles originated in convective cells, the subsequent growth of the particles in the widespread mesoscale ascent in the upper part of the nimbostratus

contributed greatly to the mass of the precipitation. In the second experiment, the vertical velocity of Figure 11b was retained, but the influx of ice particles across the right-hand wall of the domain was shut off. Without this influx of precipitable-sized ice particles, almost no rain reaches the surface at all. In this case, all ice particles had to be nucleated and grown in the nimbostratus cloud itself. They could not attain precipitable size before being advected out of the model domain.

These numerical calculations show the symbiotic relationship of the convective updrafts and the widespread ascent in the stratiform cloud region that is required to account for the precipitation that falls from nimbostratus associated with deep convection. The deep convection is essential to produce ice particles large enough to fall out within the mesoscale region of the nimbostratus, while the widespread ascent at upper levels in the nimbostratus is necessary for the particles to increase in mass before they fall out of the cloud.

8. Separation of convective and stratiform precipitation

Because of the very different dynamics and microphysics of convective and stratiform precipitation, it is important in many types of analysis to separate precipitation regions into their convective and stratiform components. When observed by radar, the precipitation can be separated into these components in two ways. If the radar beam penetrates the atmospheric volume containing the precipitation at near-vertical incidence, as would radar on board a satellite, then the existence of a radar bright band (Section 2) is a primary indicator that the precipitation is of a stratiform nature.[8] However, the bright band may not be detectable for one or more of the following reasons: (1) The precipitation layer may consistent entirely of snow. (2) The stratiform precipitation may not be intense enough to produce a strong detectable bright band. (3) The radar beam penetrates the atmospheric volume at a near horizontal angle, as is the case for most scanning radars located on the ground, ships, or aircraft. In this latter case, difficulty arises because the bright band exists only in a thin layer, and the finite beamwidth of a typical meteorological radar (~1°) scanning quasi-horizontally cannot resolve a bright band at distances from the radar where the vertical width of the beam is wider than the thickness of the bright band. Because of these difficulties in detecting the melting layer, a method must be applied to separate the stratiform radar echo from the convective echo in data obtained by radars located on the ground, ships, or aircraft that does not depend on observing the bright band.

Figure 15 illustrates a commonly used method of convective/stratiform separation that minimizes dependence of observing the bright band.[9] The technique first seeks the convective precipitation rather than the stratiform precipitation. The method is easiest to visualize if we assume that the radar echo field is expressed in a Cartesian coordinate system. Each Cartesian pixel is examined and declared a convective center if it exceeds a

---

[8] A method using the bright band as a primary indicator of stratiform precipitation in satellite radar data was introduced by Awaka et al. (1997)

[9] This method was introduced by Churchill and Houze (1984), and further developed by Steiner et al. (1997), and Yuter and Houze (1997).

prescribed threshold of reflectivity or if it exceeds the reflectivity in a region surrounding the pixel (~ 10 km in diameter) by a specified factor, which increases as the reflectivity at the convective center decreases. If a pixel is declared a convective center, then a region surrounding the convective center (usually taken to be 4-5 km in diameter) is defined as convective precipitation. No attempt is made to define a convective region smaller than 4–5 km in diameter. Often several convective centers are close together and the convective regions overlap, and the union of these convective areas may define a contiguous region of convective precipitation tens to even hundreds of kilometers across. Thus, the separation method does not attempt to identify individual up- and downdraft regions, which may be smaller in scale than 4-5 km, but rather attempts to delineate general regions of active convection, like that idealized in Figure 5a. Any pixel not identified as convective is defined as either stratiform or indeterminable. Generally most of the remaining echo is stratiform. To determine if the method is correctly identifying the remaining echo as stratiform, vertical cross sections of radar echo close to the radar, where the beam is narrow enough to resolve the bright band, are inspected to determine if the criteria chosen for determining convective echo (echo intensity, ratio of echo intensity to background echo, and width of convective area surrounding convective centers) are not accidentally including stratiform echo (e. g., if an echo identified by the algorithm as convective is found to contain a bright band). If the method is found to incorrectly categorize certain echoes, the criteria are adjusted (tuned) until vertical echo structures near the radar reliably confirm that they accurately make the separation. Finally, some echo is hard to define as either convective or stratiform, and it is filtered out by some appropriate criterion.

The method illustrated by Figure 15 is widely used and very practical because it is applied to the reflectivity field alone. Testing of the method in a situation where dual-Doppler radar data provided the vertical air motions associated with the reflectivity have confirmed that the air motions in the regions identified as convective by the reflectivity-based algorithm more vigorous in the convective than in the stratiform regions.[10]

[10] See Steiner et al. (1995) for details of this test.

Figure Captions

Figure 1 (a) Characteristics of stratiform precipitation. (b) Characteristics of convective precipitation. Shading shows higher intensities of radar echo, with the medium blue indicating the strongest echo. In (b) cloud is shown at a succession of times $t_o,\ldots,t_n$. Growing precipitation particle is carried upward by strong updrafts until t_2 and then falls relative to the ground, reaching the surface just after t_5. After t_5, the cloud may die or continue for a considerable time in a steady state before dissipation sets in at t_{n-1} and t_n. The dashed boundary indicates an evaporating cloud. (From Houze, 1981. © American Geophysical Union.)

Figure 2 Schematic of vertical profile of radar data in stratiform precipitation. Solid curve shows reflectivity. Dashed curve shows Doppler radial velocity V_R with the antenna at vertical incidence. Under stratiform conditions V_R is related approximately to the mass-weighted terminal fall speed of the particles, $\hat{V}$. Points 0-4 bound the layers in which different microphysical processes dominate (see text for further discussion).

Figure 3 Ice particle data obtained on aircraft flights through nimbostratus in tropical mesoscale convective systems over the Bay of Bengal. Plots show relative frequency of observation of ice particles of a particular type per minute of in-cloud flight time as a function of flight-level temperature. (From Houze and Churchill, 1987. Reproduced with permission from the American Meteorological Society.)

Figure 4 **(previously Figure 12YH95C)** Conceptual model of a buoyant updraft element. Dots indicate hydrometeors suspended by updraft; downward-pointing arrows indicate particles heavy enough to fall through updraft; horizontal arrows indicate lateral spreading of bubble. Open arrows represent the vector field of the buoyancy pressure gradient force (From Yuter and Houze, 1995c. Reprinted with permission from the American Meteorological Society.)

Figure 5 Conceptual models of vertical cross sections through idealized young, vigorous precipitating convection with no environmental shear. (From Houze, 1997. Reprinted with permission from the American Meteorological Society.)

Figure 6 Conceptual models of vertical cross sections of old convection that has taken on a stratiform structure. (From Houze, 1997. Reprinted with permission from the American Meteorological Society.)

Figure 7 Conceptual model of the development of nimbostratus associated with deep convection. Panels (a), (c), and (e) show horizontal radar echo pattern at the earth's surface with two levels of intensity at three times, t_o, $t_o + \Delta t$, and $t_o + 2\Delta t$. Panels (b), (d), and (f) show corresponding vertical cross sections. A sketch of the visible cloud boundary has been added to the vertical cross sections. Asterisks trace the fallout of three ice particles.

Figure 8 Conceptual model of an ensemble of particle fountains in a multicellular MCS. Shaded area represents radar reflectivity along a cross section perpendicular to the convective region. Cloud boundary is indicated by the scalloped outline. Inset shows approximate scales and arrangement of the largest particle fountains relative to the radar echo. (From Yuter and Houze, 1995c. Reprinted with permission from the American Meteorological Society.)

Figure 9 Schematic of the precipitation mechanisms in a mesoscale convective system. Solid arrows indicate particle trajectories. (From Houze, 1989. Reprinted with permission from the Royal Meteorological Society.)

Figure 10 Schematic of convective evolution over the near-equatorial Indian Ocean. An eastward moving convergence line triggers convection, and lower tropospheric winds advect the new boundary-layer rooted convection eastward. Upper-level winds advect the stratiform cloud and precipitation formed as the convection matures to the east, where it intercepts new convection formed to its west. (Adapted from Yamada et al. 2010. Reprinted with permission from the American Meteorological Society.)

Figure 11 Horizontal wind and vertical air motion assumed to exist in the domain of a numerical simulation of a stratiform region. Deep convection is assumed to be located immediately to the right of the domain. Data are from a squall-line mesoscale convective system observed over Oklahoma. (From Rutledge and Houze, 1987. Reprinted with permission from the American Meteorological Society.)

Figure 12 The steady-state distributions of mixing ratios of (a) snow q_s, (b) graupel q_g, and (c) rainwater q_r in a numerical simulation of a stratiform region associated with deep convection located immediately to the right of the domain of the calculations. Units are g kg^{-1}. (From Rutledge and Houze, 1987. Reprinted with permission from the American Meteorological Society.)

Figure 13 As in Figure 12 except for (a) rain rate (mm h^{-1}) and (b) radar reflectivity (dBZ). (From Rutledge and Houze, 1987. Reprinted with permission from the American Meteorological Society.)

Figure 14 As in Figure 12 except for (a) depositional growth rate of less dense snow, (b) depositional growth rate of more dense snow, (c) melting rate, and (d) rate of evaporation of rain. Units are 10^{-3} g kg^{-1} s^{-1}. (Courtesy of S. A. Rutledge.)

Figure 15 Schematic illustrating a method for separating the convective component of precipitation from the rest of the precipitation. The illustration assumes 2-km Cartesian grid spacing for the data points; however, the method may be applied at different resolutions and could be adapted to polar coordinates. The algorithm examines the reflectivity at each grid point. If that reflectivity exceeds some prescribed high value, or if it exceeds the mean reflectivity in a "background region" (lightly shaded region, ~ 10 km in diameter) surrounding the point by

some specified amount, the point is declared a convective center. If the point is declared a convective center, then that point and all the points in a small region (~ 4–5 km in diameter) surrounding the convective center constitute a “convective region” centered on the point. This exercise is repeated for each data point in the grid and the union of all the convection regions makes up the total convective precipitation region. (From Houze, 1997. Reprinted with permission from the American Meteorological Society.)

References

Awaka J., T. Iguchi, H. Kumagai, and K. Okamoto, 1997: Rain type classification algorithm for TRMM precipitation radar. *Proc. IEEE 1997 Int. Geoscience and Remote Sensing Symp.,* Singapore, Japan, Institute of Electrical and Electronics Engineers, 1633-1635.

Battan, L. J., 1959: *Radar Meteorology*. University of Chicago Press, Chicago, 161 pp.

Battan, L. J., 1973: *Radar Observations of the Atmosphere*. University of Chicago Press, Chicago, 324 pp.

Bergeron, T., 1950: Über der Mechanismus der ausgiebigan Neiderschläge. *Ber. deutsch. Wetterd.*, **12**, 225-232.

Biggerstaff, M. I., and R. A. Houze, Jr., 1993: Kinematics and microphysics of the transition zone of the 10-11 June 1985 squall-line. *J. Atmos. Sci.*, **50**, 3091-3110.

Braun, S. A., and R. A. Houze, Jr., 1994: The transition zone and secondary maximum of radar reflectivity behind a midlatitude squall line: Results retrieved from Doppler radar data. Accepted, *J. Atmos. Sci.*

Businger, S., and P. V. Hobbs, 1987: Mesoscale structures of two comma cloud systems over the Pacific Ocean. *Mon. Wea. Rev.*, **115**, 1908-1928.

Churchill, D. D., and R. A. Houze, Jr., 1991: Effects of radiation and turbulence on the diabatic heating and water budget of the stratiform region of a tropical cloud cluster. *J. Atmos. Sci.*, **48,** 903–922.

Hobbs, P. V., T. J. Matejka, P. H. Herzegh, J. D. Locatelli and R. A. Houze, Jr., 1980: The mesoscale and microscale structure and organization of clouds and precipitation in midlatitude cyclones. I: A case study of a cold front. J. Atmos. Sci., **37**, 568-596.

Houghton, H. G., 1968: On precipitation mechanisms and their artificial modification. *J. Appl. Meteor.*, **7,** 851–859.

Houze, R. A., Jr., 1981: Structure of atmospheric precipitation systems—A global survey, *Radio Science, 16,* 671-689.

Houze, R. A., Jr., 1989: Observed structure of mesoscale convective systems and implications for large-scale heating. *Quart. J. Roy. Met. Soc.*, **115,** 425–461.

Houze, R. A., Jr., 1997. Stratiform precipitation in regions of convection: a meteorological paradox? *Bull. Amer. Meteor. Soc.* **78**: 2179-2196.

Houze, R. A., Jr., and D. D. Churchill, 1987: Mesoscale organization and cloud microphysics in a Bay of Bengal depression. *J. Atmos. Sci.*, **44**, 1845-1867.

Houze, R. A., Jr., S. A. Rutledge, T. J. Matejka, and P. V. Hobbs, 1981: The mesoscale and microscale structure and organization of clouds and precipitation in midlatitude cyclones. III: Air motions and precipitation growth in a warm-frontal rainband. *J. Atmos. Sci.,* **38**, 639-649.

Ligda, M. G. H., 1956: The radar observations of mature prefrontal squall lines in the midwestern United States. *VI Congress of Organisation Scientifique et Technique Internationale du Vol a Voile (OSTIV)*, Aeronautical International Federation, St-Yan, France, 6-14 July, Publication IV, pp. 1-3.

Marshall, J. S., 1953: Frontal precipitation and lightning observed by radar. *Can. J. Phys.*, **31,** 194–203.

Rutledge, S. A., and P. V. Hobbs, 1983: The mesoscale and microscale structure and organization of clouds and precipitation in midlatitude cyclones. VIII: A model for the feeder–seeder process in warm frontal rainbands. *J. Atmos. Sci.*, **40,** 1185–1206.

Rutledge, S. A., and R. A. Houze, Jr., 1987: A diagnostic modeling study of the trailing stratiform region of a midlatitude squall line. *J. Atmos. Sci*., **44,** 2640–2656.

Steiner, M., R. A. Houze, Jr., and S. E. Yuter, 1995: Climatological characterization of three-dimensional storm structure from operational radar and rain gauge data. *J. Appl. Meteor.,* **34,** 1978-2007.

Yamada, H., K. Yoneyama, M. Katsumata, and R. Shirooka, 2010: Observations of a super cloud cluster accompanied by synoptic-scale eastward-propagating precipitating systems over the Indian Ocean. *J. Atmos. Sci*., **67**, 1456–1473.

Yuter, S. E. and R. A. Houze, Jr., 1995b: Three-dimensional kinematic and microphysical evolution of Florida cumulonimbus. Part II: Frequency distributions of vertical velocity, reflectivity, and differential reflectivity. *Monthly Weather Review*, **123**, 1941-1963.

Yuter, S. E., and R. A. Houze, Jr., 1995c: Three-dimensional kinematic and microphysical evolution of Florida cumulonimbus. Part III: Vertical mass transport, mass divergence, and synthesis. *Mon. Wea. Rev.,* **123**, 1964-1983.

Yuter, S. E., and R. A. Houze, Jr., 1997: Measurements of raindrop size distributions over the Pacific warm pool and implications for Z-R relations. *J. Appl. Meteor*., **36**, 847-867.

Wallace, J. M., and P. V. Hobbs, 2006: *Atmospheric Science: An Introductory Survey*. 2nd Ed., Academic Press, New York, 483 pp.

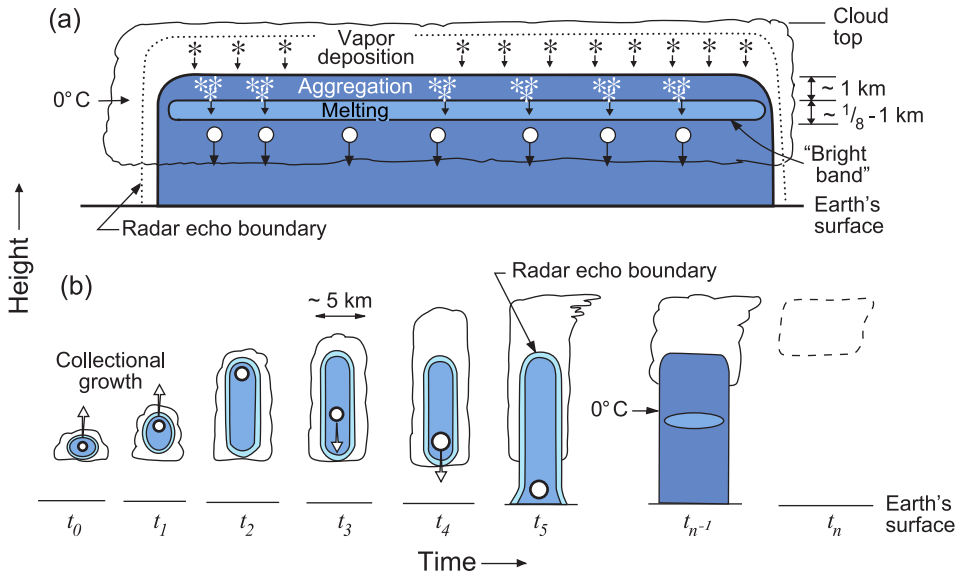

Figure 1 (a) Characteristics of stratiform precipitation. (b) Characteristics of convective precipitation. Shading shows higher intensities of radar echo, with the medium blue indicating the strongest echo. In (b) cloud is shown at a succession of times t_o,…,t_n. Growing precipitation particle is carried upward by strong updrafts until t_2 and then falls relative to the ground, reaching the surface just after t_5. After t_5, the cloud may die or continue for a considerable time in a steady state before dissipation sets in at t_{n-1} and t_n. The dashed boundary indicates an evaporating cloud. (From Houze, 1981. © American Geophysical Union.)

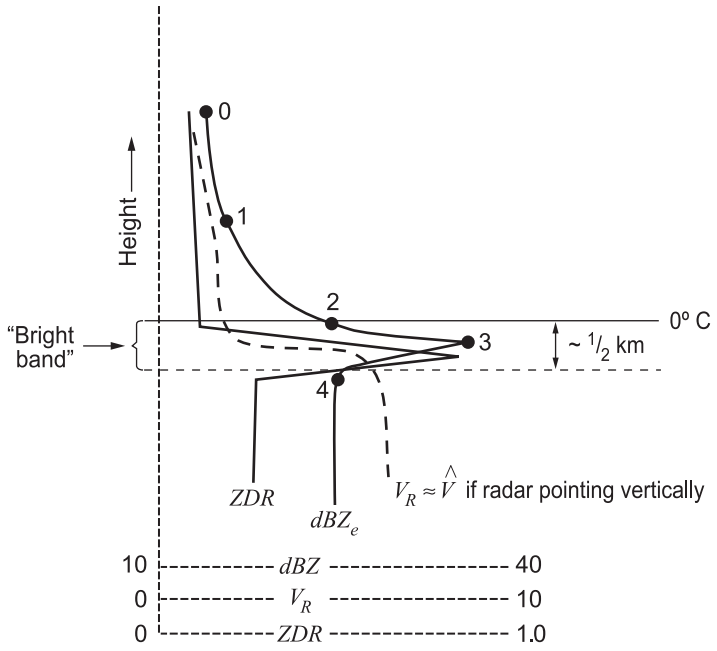

Figure 2 Schematic of vertical profile of radar data in stratiform precipitation. Solid curve shows reflectivity. Dashed curve shows Doppler radial velocity V_R with the antenna at vertical incidence. Under stratiform conditions V_R is related approximately to the mass-weighted terminal fall speed of the particles, $\hat{V}$. Points 0-4 bound the layers in which different microphysical processes dominate (see text for further discussion).

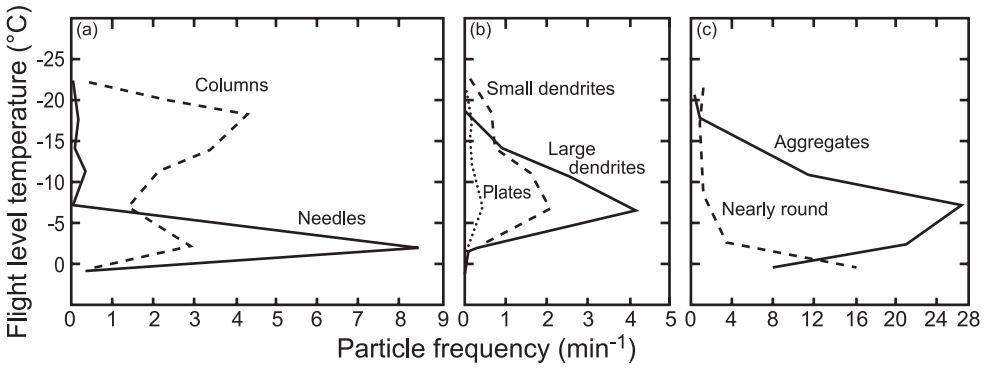

Figure 3 Ice particle data obtained on aircraft flights through nimbostratus in tropical mesoscale convective systems over the Bay of Bengal. Plots show relative frequency of observation of ice particles of a particular type per minute of in-cloud flight time as a function of flight-level temperature. (From Houze and Churchill, 1987. Reproduced with permission from the American Meteorological Society.)

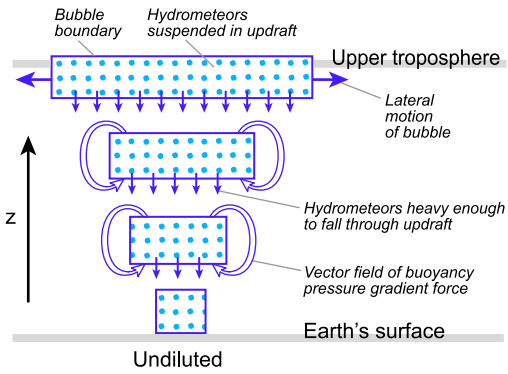

Figure 4 Conceptual model of a buoyant updraft element. Dots indicate hydrometeors suspended by updraft; downward-pointing arrows indicate particles heavy enough to fall through updraft; horizontal arrows indicate lateral spreading of bubble. Open arrows represent the vector field of the buoyancy pressure gradient force (From Yuter and Houze, 1995c. Reprinted with permission from the American Meteorological Society.)

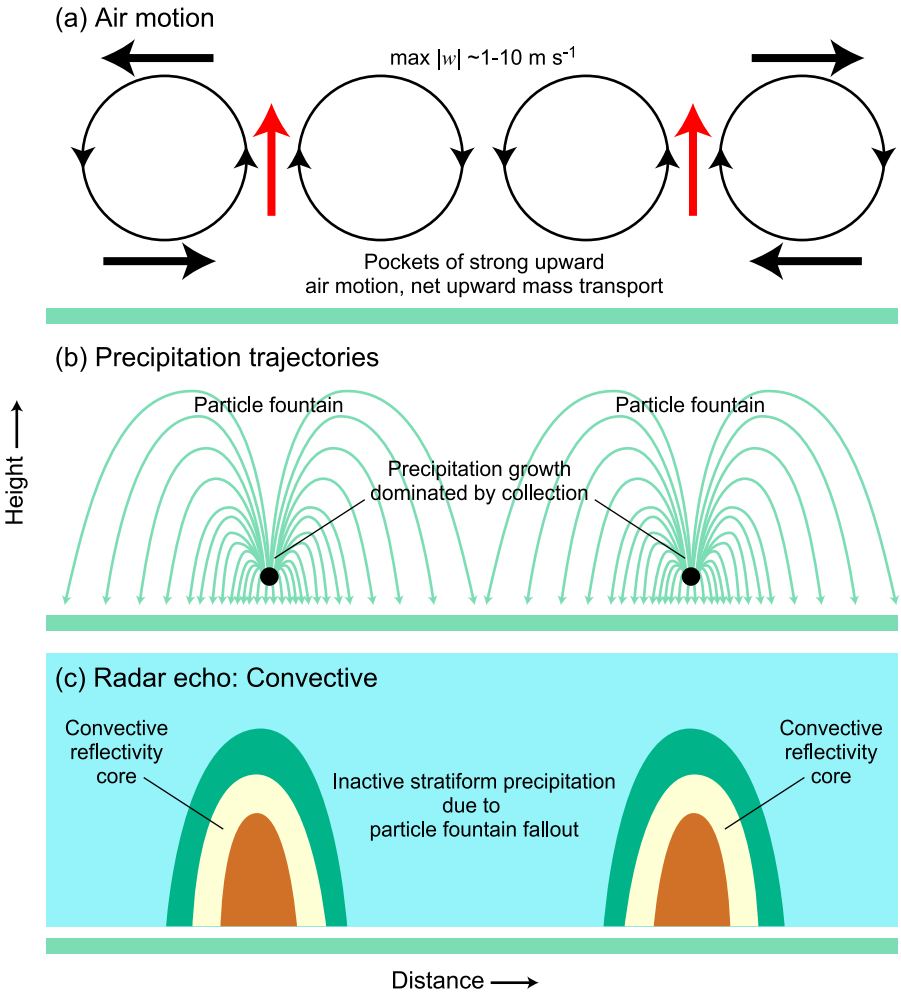

Figure 5 Conceptual models of vertical cross sections through idealized young, vigorous precipitating convection with no environmental shear. (From Houze, 1997. Reprinted with permission from the American Meteorological Society.)

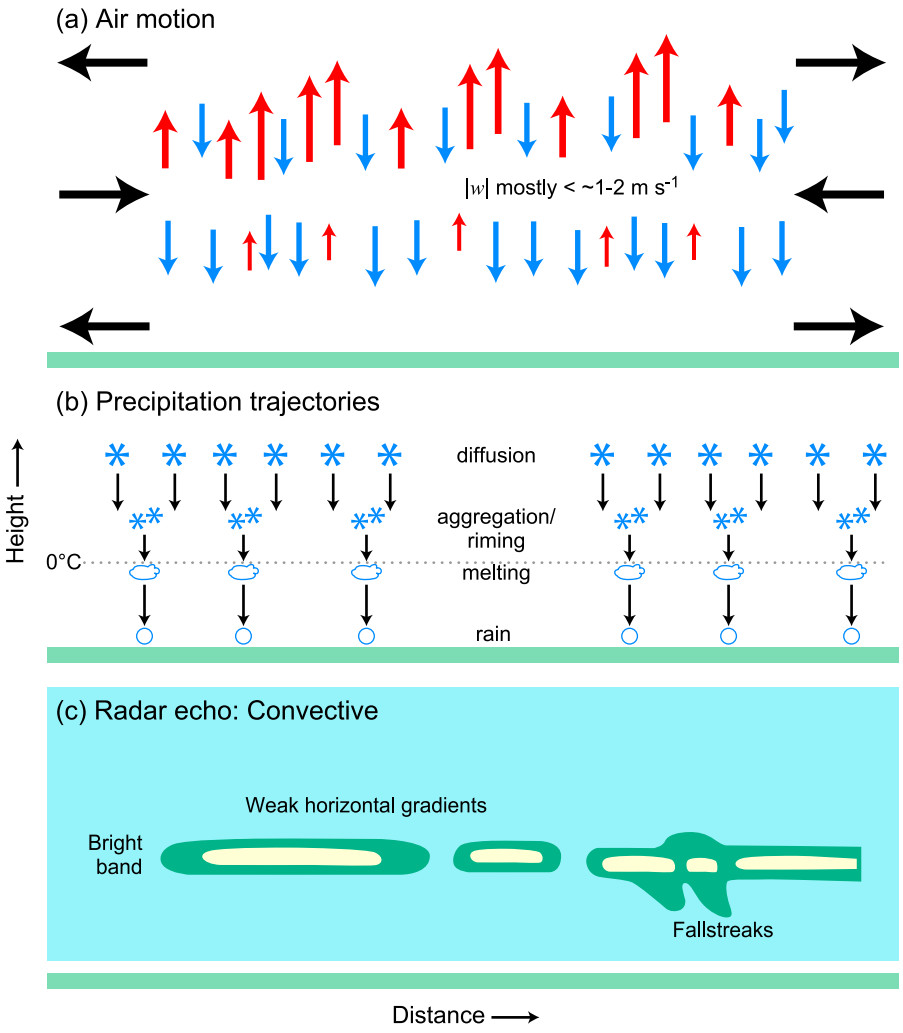

Figure 6 Conceptual models of vertical cross sections of old convection that has taken on a stratiform structure. (From Houze, 1997. Reprinted with permission from the American Meteorological Society.)

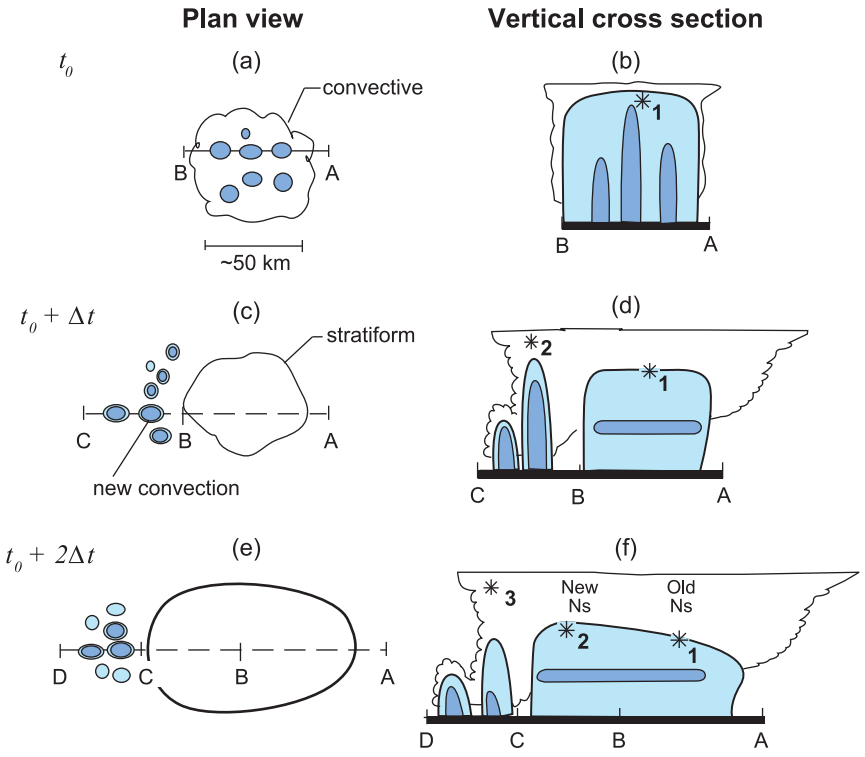

Figure 7 Conceptual model of the development of nimbostratus associated with deep convection. Panels (a), (c), and (e) show horizontal radar echo pattern at the earth's surface with two levels of intensity at three times, t_o, $t_o + \Delta t$, and $t_o + 2\Delta t$. Panels (b), (d), and (f) show corresponding vertical cross sections. A sketch of the visible cloud boundary has been added to the vertical cross sections. Asterisks trace the fallout of three ice particles.

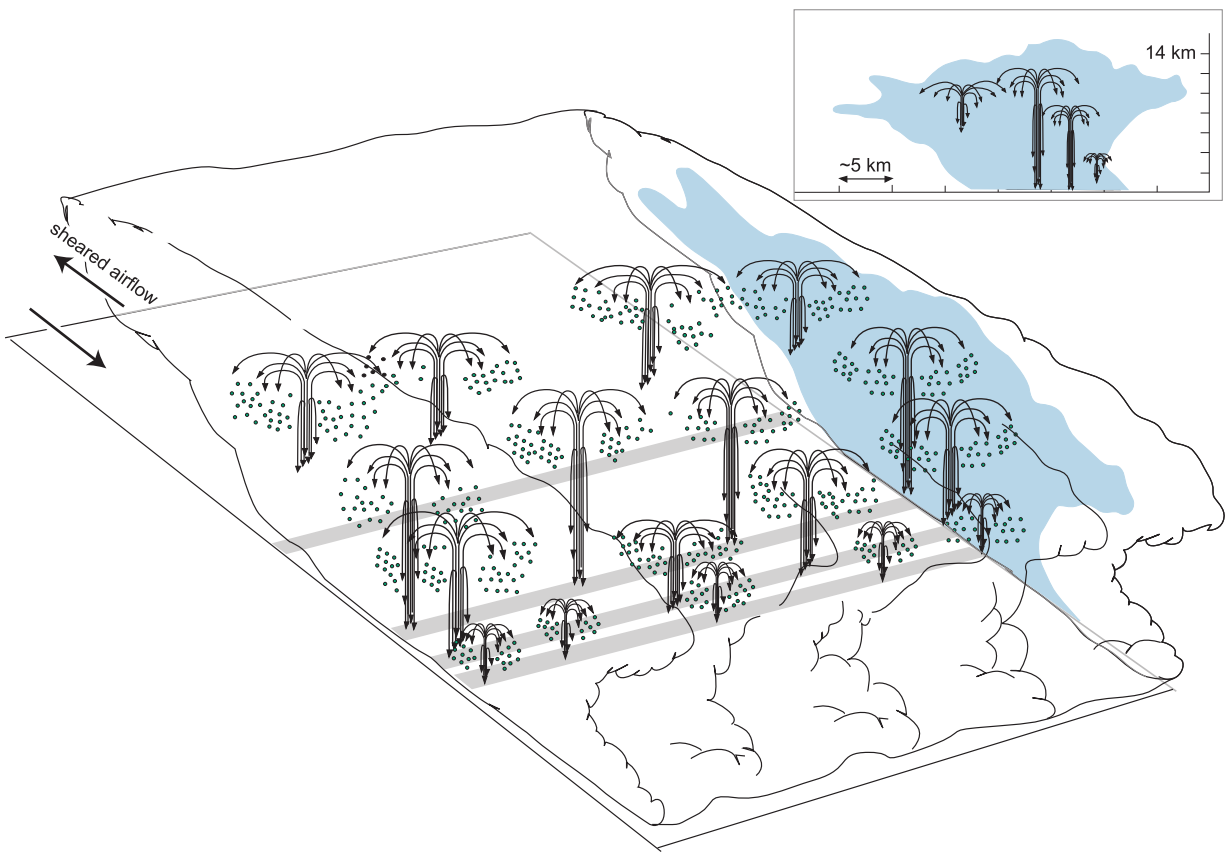

Figure 8 Conceptual model of an ensemble of particle fountains in a multicellular MCS. Shaded area represents radar reflectivity along a cross section perpendicular to the convective region. Cloud boundary is indicated by the scalloped outline. Inset shows approximate scales and arrangement of the largest particle fountains relative to the radar echo. (From Yuter and Houze, 1995c. Reprinted with permission from the American Meteorological Society.)

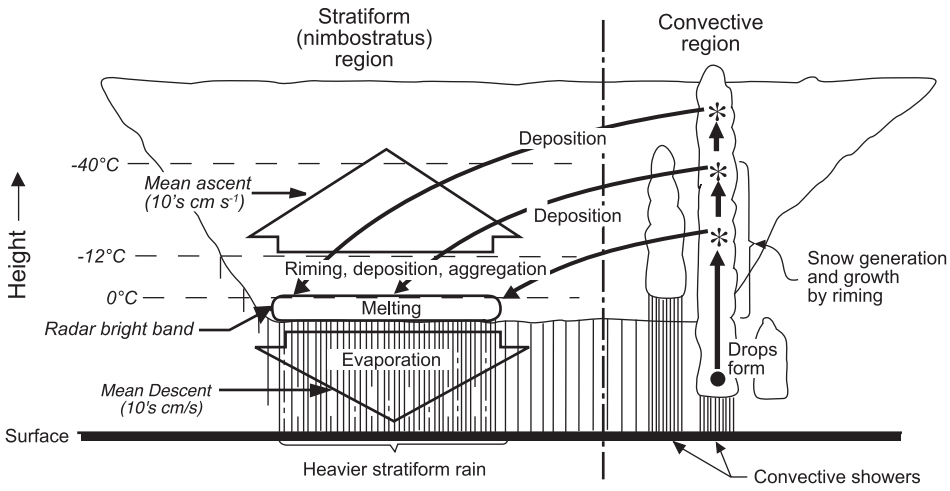

Figure 9 Schematic of the precipitation mechanisms in a mesoscale convective system. Solid arrows indicate particle trajectories. (From Houze, 1989. Reprinted with permission from the Royal Meteorological Society.)

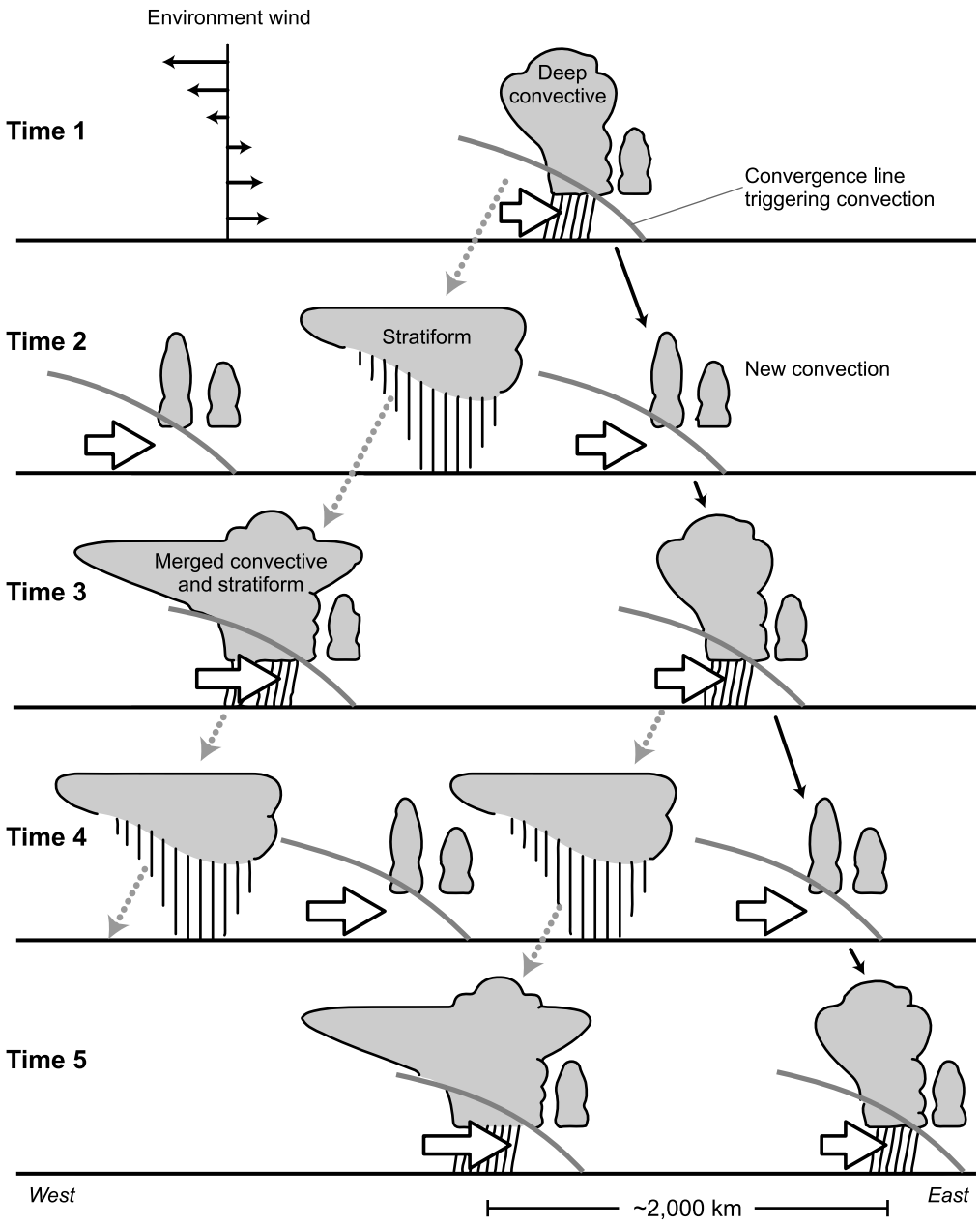

Figure 10 Schematic of convective evolution over the near-equatorial Indian Ocean. An eastward moving convergence line triggers convection, and lower tropospheric winds advect the new boundary-layer rooted convection eastward. Upper-level winds advect the stratiform cloud and precipitation formed as the convection matures to the east, where it intercepts new convection formed to its west. (Adapted from Yamada et al. 2010. Reprinted with permission from the American Meteorological Society.)

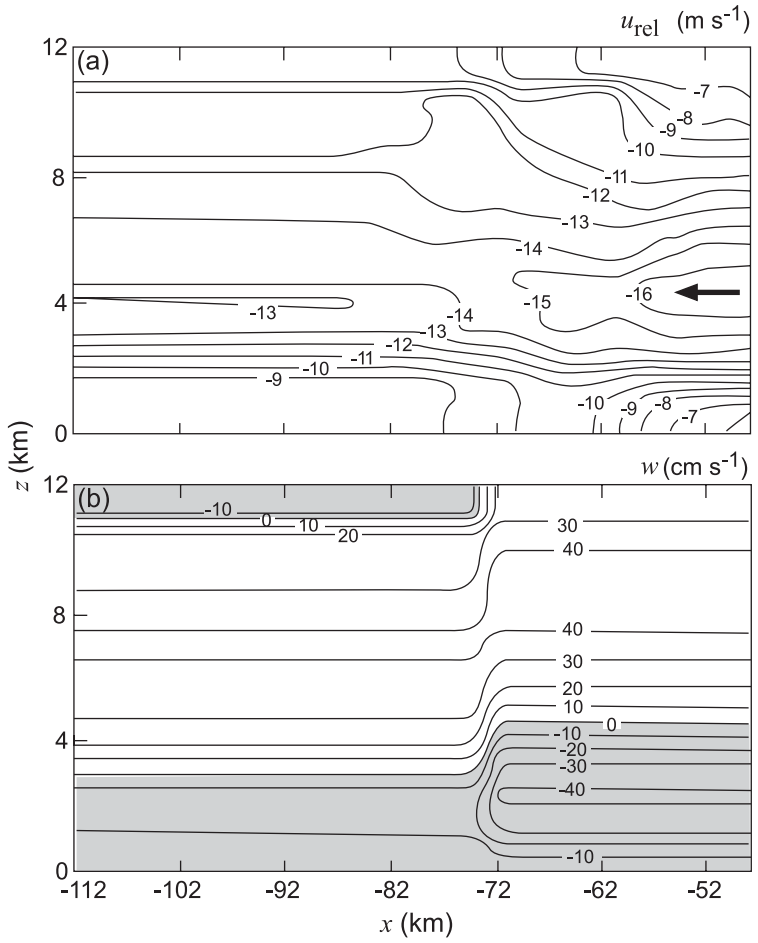

Figure 11 Horizontal wind and vertical air motion assumed to exist in the domain of a numerical simulation of a stratiform region. Deep convection is assumed to be located immediately to the right of the domain. Data are from a squall-line mesoscale convective system observed over Oklahoma. (From Rutledge and Houze, 1987. Reprinted with permission from the American Meteorological Society.)

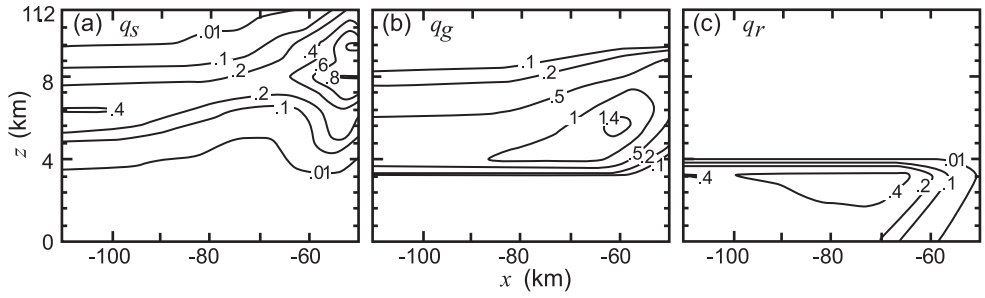

Figure 12 The steady-state distributions of mixing ratios of (a) snow q_s, (b) graupel q_g, and (c) rainwater q_r in a numerical simulation of a stratiform region associated with deep convection located immediately to the right of the domain of the calculations. Units are g kg^{-1}. (From Rutledge and Houze, 1987. Reprinted with permission from the American Meteorological Society.)

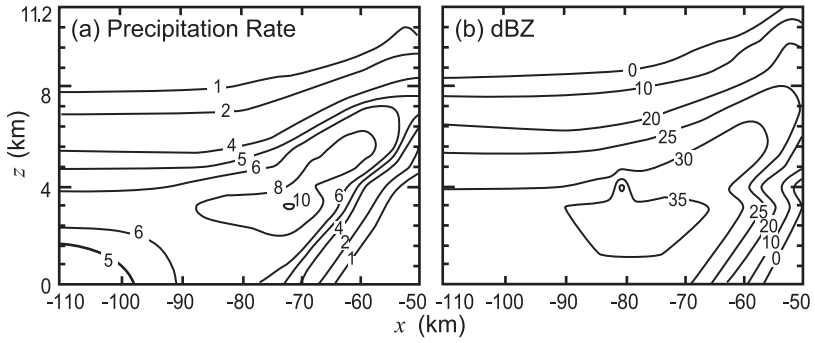

Figure 13 As in Figure 12 except for (a) rain rate (mm h^{-1}) and (b) radar reflectivity (dBZ). (From Rutledge and Houze, 1987. Reprinted with permission from the American Meteorological Society.)

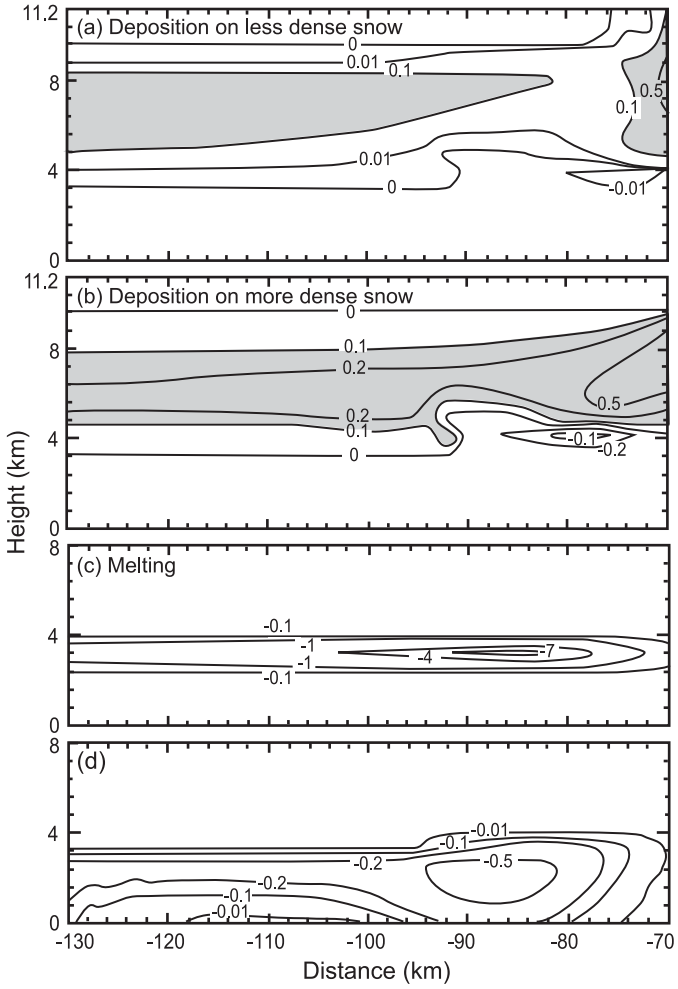

Figure 14 As in Figure 12 except for (a) depositional growth rate of less dense snow, (b) depositional growth rate of more dense snow, (c) melting rate, and (d) rate of evaporation of rain. Units are 10^{-3} g kg^{-1} s^{-1}. (Courtesy of S. A. Rutledge.)

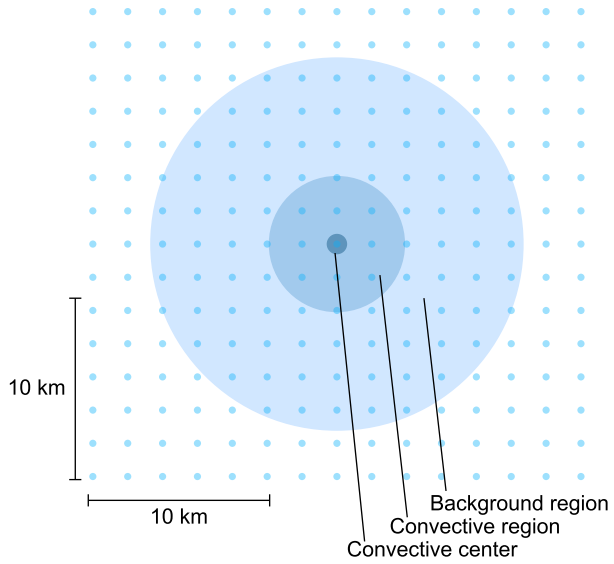

Figure 15 Schematic illustrating a method for separating the convective component of precipitation from the rest of the precipitation. The illustration assumes 2-km Cartesian grid spacing for the data points; however, the method may be applied at different resolutions and could be adapted to polar coordinates. The algorithm examines the reflectivity at each grid point. If that reflectivity exceeds some prescribed high value, or if it exceeds the mean reflectivity in a "background region" (lightly shaded region, ~ 10 km in diameter) surrounding the point by some specified amount, the point is declared a convective center. If the point is declared a convective center, then that point and all the points in a small region (~ 4–5 km in diameter) surrounding the convective center constitute a "convective region" centered on the point. This exercise is repeated for each data point in the grid and the union of all the convection regions makes up the total convective precipitation region. (From Houze, 1997. Reprinted with permission from the American Meteorological Society.)